A mathematical model for a plasma-assisted downstream etching reactor

Sang-Kyu Park and Demetre J. Economou[a]

Department of Chemical Engineering, University of Houston, Houston, Texas 77204-4792

A mathematical model was developed for a plasma-assisted downstream etching reactor of the impinging jet configuration. Finite-element methods were employed to solve for the two-dimensional fluid velocity, temperature, and active species concentration distributions. Etching of a polymer (e.g., photoresist) using pure oxygen was analyzed with emphasis on the effect of reactor design and operating conditions on etching rate and uniformity. For a given flow rate, an optimum value of pressure was identified which maximized the etching rate. The etching rate increased monotonically with power, but decreased exponentially with distance between the plasma and the wafer. Under the conditions examined, the etching rate was found to be highest at the wafer center. Local loading was observed around the periphery of the wafer at high wafer temperature. The etching uniformity was found to depend on the gas-flow distribution. A new reactor design was proposed to achieve efficient gas dissociation in the plasma, rapid transport of the dissociated gas to the etching chamber, and nearly uniform flow distribution over the wafer. The new design resulted in improvement in both etching rate and uniformity.

I. INTRODUCTION

Plasma-assisted etching is a critical step in microelectronic device fabrication, especially when delineation of micrometer-size patterns is required. However, as device dimensions continue to shrink, minimization of the "damage" caused by harmful plasma radiation on sensitive devices becomes increasingly important.[1,2] For example, in the fabrication of advanced memory devices, removal of ion-implantation-hardened resists off thin gate oxides often results in oxide damage when the resist is exposed directly to the plasma.[3,4] Plasma-assisted downstream etching (PADE) techniques have recently received attention as a method to minimize the radiation damage.[5] In this method, the plasma is usually excited in an electrodeless discharge cavity using a microwave or rf power source. Active species created in the plasma cavity are then transported by gas flow downstream in the etching chamber housing the substrate. Under appropriate conditions, the exposure of the substrate to energetic ions, electrons, or photons originating from the plasma can be minimal. Such conditions minimize or eliminate radiation damage. Other advantages of PADE are high reaction selectivity, since etching is purely chemical without any ion bombardment effects, and greater process flexibility. However, the absence of ion bombardment results in isotropic etching. Furthermore, end-point detection may be difficult in PADE.

PADE has been utilized for etching of photoresist and other polymeric films using O_2 or O_2/fluorocarbon discharges,[6-10] as well as for etching of various thin films.[11-13] A variation of downstream etching is the so-called plasma stream etching method utilizing an electron cyclotron resonance (ECR) plasma source.[14] In this method the operating pressure is relatively low ($p < 10^{-3}$ Torr) and the substrate is exposed to a low-energy ion bombardment. In addition to etching, plasma-assisted downstream methods are gaining popularity in thin-film deposition. For example, such methods have been used for the deposition of Si and Ge films[15,16] as well as diamondlike films.[17]

The central goals of plasma-assisted downstream etching are high etching rate and uniformity and no radiation damage. Owing to the complexity of the system and the large number of variables involved, pursuing the above goals based solely on intuition and trial-and-error experimentation can be time consuming and costly. Mathematical models based on first principles can assist in identifying the optimum reactor design and operating conditions.

Although PADE has been used for some time, especially for photoresist stripping, there is no theoretical work analyzing the effect of reactor design and operating conditions on the etching rate and uniformity achieved. The purpose of this work is to develop a mathematical model based on transport and reaction principles to analyze a plasma-assisted downstream etching reactor. The effect of process variables on etching rate and uniformity is emphasized. Changes in the reactor design and their effect on etching rate and uniformity are also examined. Polymer (e.g., photoresist) etching using an oxygen plasma in an impinging jet reactor configuration was selected as a model system for study. This selection was based on the fact that photoresist stripping is currently the main application of PADE, and that the oxygen plasma system is relatively better understood.[18,19] The mathematical model is described in Sec. II, and the method of solution is outlined in Sec. III. Section IV contains the results and discussion, and Sec. V contains the summary and conclusions.

II. MODEL FORMULATION

A schematic of the plasma-assisted downstream etching reactor studied is shown in Fig. 1. The axisymmetric reactor

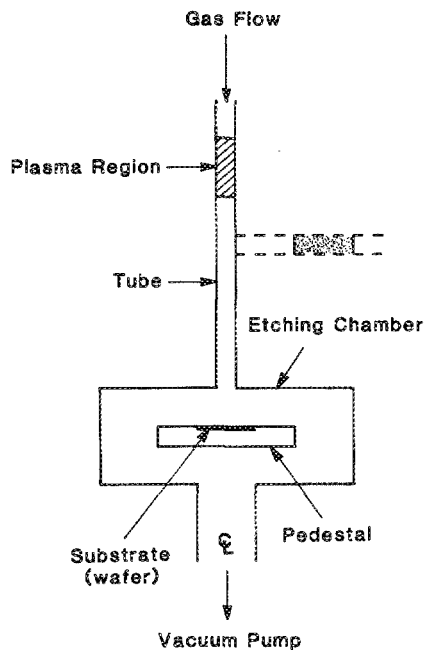[a] Author to whom all correspondence should be addressed.

FIG. 1. Schematic of the plasma-assisted downstream etching (PADE) reactor studied. Dashed line shows "angled" configuration to avoid line-of-sight communication between the plasma and the substrate.

consists of a tube (e.g., made of quartz) leading to a cylindrical etching chamber. The substrate (e.g., semiconductor wafer) rests on a temperature-controlled pedestal in the etching chamber. The plasma region extends over a certain length along the tube. The plasma may be created by a microwave discharge cavity or by a rf source. An otherwise inert gas is fed to the tube inlet and passes through the plasma region where reactive species are produced. The "activated" gas flows downstream and encounters the substrate in an impinging jet flow configuration. Etching reaction products and unreacted gases are pumped uniformly from below the pedestal. The above reactor configuration is similar to the one used for experimental work by Vukanovic et al.[8]

In order to avoid exposure of the substrate to energetic plasma particles, the plasma cavity must be at a sufficient distance from the substrate. Further, exposure of the substrate to harmful photon radiation may be minimized by configuring the plasma so as to avoid direct line-of-sight communication between the plasma and the substrate. An example of such configuration is shown by the dashed line in Fig. 1. In the present work such "angled" configuration was not considered in order to preserve the axisymmetric geometry which leads to substantial computational savings. Nevertheless, if the effect of photons on the surface reaction rate is not significant, similar results on etching rate and uniformity are expected with the two reactor configurations.

Modeling of a PADE reactor requires consideration of the glow-discharge (plasma) physical chemistry and of the transport and reaction phenomena in both the plasma region and the downstream region, including the etching chamber. Moreover, information about the etching reaction kinetics is needed. Such phenomena are described in the following paragraphs for the stripping of photoresist using pure oxygen. The dimensions of the system studied are shown in Fig. 2(b), and parameter values are included in Tables I and II.
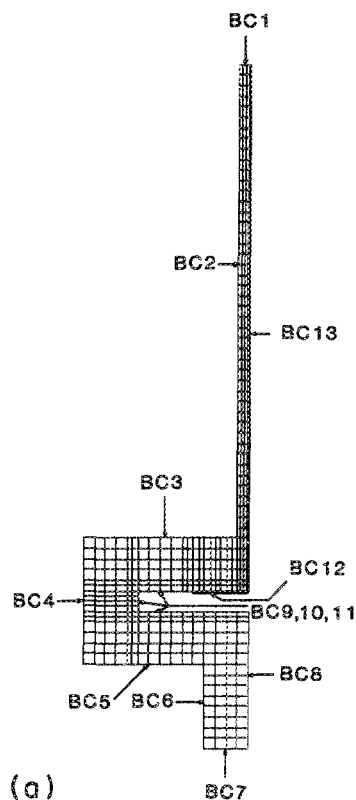

(a)

(b)

FIG. 2. (a) Finite-element mesh used for most calculations. BC No. indicates the surface on which the corresponding boundary condition was applied. (b) Dimensions of the PADE reactor studied. H_{ps} and H_{ts} were varied. Solid line shows the basic reactor design, dashed line shows the reactor with tapered wall, and dash-dotted line shows the reactor with a 2-cm radius of the plasma region.
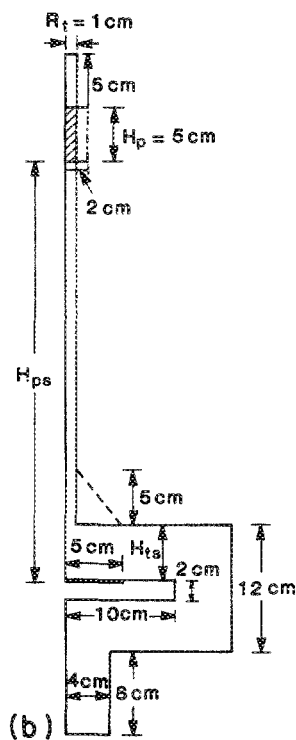
TABLE I. Parameter basic values and range examined.

Symbol	Name	Basic value	Range examined
H_{ps}	Plasma end to substrate distance	40 cm	10–40 cm
H_{ts}	Tube end to substrate distance	5 cm	1–5 cm
P	Plasma power	50 W	25–300 W
p	Gas pressure	1 Torr	0.5–3 Torr
Q_0	Inlet gas-flow rate	100 sccm	50–1000 sccm
T_s	Substrate (wafer) temperature	373 K	373–513 K

A. The plasma cavity

The plasma is the source of etchant species such as atomic oxygen. Power from a high-frequency source is coupled to the flowing gas leading to dissociation and ionization of parent oxygen molecules. Owing to the electrodeless nature of the discharge, much of the ionization occurs in the bulk plasma and the discharge may resemble a positive column.[20,21] The effective electric field E_{eff} approximation may then be used to describe the discharge. The effective electric-field-to-pressure ratio E_{eff}/p was estimated as a function of $p\Lambda$, where p is the gas pressure, and Λ is the electron diffusion length given by

$$\frac{1}{\Lambda^2} = \left(\frac{2.405}{R_t}\right)^2 + \left(\frac{\pi}{H_p}\right)^2, \tag{1}$$

where R_t is the tube radius and H_p is the plasma length. For given plasma dimensions, pressure, and power input, the average electron density n_e was estimated from data for a pure oxygen discharge using[18,22]

$$\frac{P}{v_p} = \frac{n_e e^2 E_{eff}^2}{m v_e}, \tag{2}$$

TABLE II. Other parameter values. These parameters were not varied.

Symbol	Name	Value
T_0	Inlet gas temperature	298 K
T_w	Reactor wall temperature	298 K
R_S	Substrate (wafer) radius	5 cm
R_p	Substrate holder (pedestal) radius	10 cm
R_t	Tube radius	1 cm
H_p	Length of plasma cavity	5 cm
E	Etching reaction activation energy	10.7 kcal/mol
k_{n0}	Preexponential factor of etching reaction rate constant	2.8×10^7 cm/s
k_1	Volume recombination rate constant	4.782×10^{14} cm^6/mol^2 s
k_2	Volume recombination rate constant	8.343×10^{14} cm^6/mol^2 s
k_3	Volume recombination rate constant	5.441×10^{13} cm^6/mol^2 s
γ	Wall recombination coefficient	1.6×10^{-4} at 298 K (T dependent)

where P is the power dissipated in the discharge, v_p is the discharge volume ($v_p = \pi R_t^2 H_p$), e is the electronic charge, m is the electron mass, and v_e is the electron momentum transfer collision frequency.

The degree of gas dissociation depends on the electron density and electron energy distribution function (EEDF), the gas pressure and flow rate, and the tube wall material. The EEDF generally depends on the discharge operating conditions such as pressure and excitation frequency. In the present work, a Maxwellian EEDF was assumed. However, the model can include other forms of the EEDF such as a Druyvesteyn distribution, or a more general form of the EEDF.[23,24]

With E_{eff}/p known, the average electron energy and electron transport and reaction coefficients may be determined. For example, for a Maxwellian EEDF, the rate constant k_p for the dissociation reaction

$$O_2 + e \xrightarrow{k_p} 2O + e, \tag{3}$$

may be found by

$$k_p = \sqrt{\frac{8}{\pi m}}(kT_e)^{-3/2} \int_0^\infty \epsilon \sigma_p(\epsilon) \exp\left(-\frac{\epsilon}{kT_e}\right) d\epsilon, \tag{4}$$

where k is the Boltzmann constant, ϵ is the electron energy, $\sigma_p(\epsilon)$ is the reaction cross section, and T_e is the electron temperature.

The gas leaving the plasma region contains a variety of species such as molecular and atomic oxygen at ground as well as excited states, electrons, and positive and negative ions. However, this "activated" gas quickly deactivates in the afterglow region and only species with a long lifetime remain to be transported downstream into the etching chamber.

B. Fluid flow and heat transport

Under the conditions of interest, the pressure is high enough for the continuum approximation to be valid, and the flow is laminar and axisymmetric. The velocity field was obtained by solving the steady-state Navier–Stokes equations

$$\rho_0 \mathbf{v} \cdot \nabla \mathbf{v} = \nabla \cdot \tau + \rho_0 \mathbf{g} \beta(T - T_0), \tag{5}$$

where the tensor

$$\tau = -p\mathbf{I} + \mu[\nabla \mathbf{v} + (\nabla \mathbf{v})^T], \tag{6}$$

I being the identity matrix, along with the continuity equation

$$\nabla \cdot \mathbf{v} = 0. \tag{7}$$

Here $\mathbf{v}$ is the fluid velocity vector, ρ and μ are the fluid density and viscosity, respectively, p is pressure, T is gas temperature, g is the gravitational acceleration vector, subscript 0 refers to a reference temperature (298 K), and β is the thermal expansion coefficient given by

$$\beta = \frac{1}{V}\left(\frac{\partial V}{\partial T}\right)_p. \tag{8}$$

The usual Boussinesq approximation was applied which

treats density as a constant in all terms of the governing equations except for the buoyancy term[25] [last term in Eq. (5)]. This approximation seems appropriate for the system at hand since the temperature variations in the reactor are relatively small.

The gas temperature distribution was obtained by solving

$$\rho c_p (\mathbf{v} \cdot \nabla T) = \nabla \cdot (\kappa \nabla T) + G_h, \tag{9}$$

where c_p is the constant pressure heat capacity, κ is the gas thermal conductivity, and G_h is the heat generation rate per unit volume. The latter can account for the fraction of the power put into the plasma which is dissipated to gas heating, or for the heat released by volume reactions, such as volume recombination of active species. For the low-pressure and power conditions examined in this work, G_h is rather small and may be neglected. The fluid flow and heat transport equations are coupled through the temperature dependence of gas viscocity and through the buoyancy term.

The following boundary conditions on fluid velocity and temperature were used, where the boundary condition (BC) number refers to the corresponding surface as shown in Fig. 2(a):
BC1:

$$v_z = 2v_{avg} [1 - (r^2/R_i^2)], \quad v_r = 0, \quad T = T_0; \tag{10}$$

BC2–6:

$$v_z = v_r = 0, \quad T = T_w; \tag{11}$$

BC 7,8,13:

$$\frac{\partial v_z}{\partial n} = 0, \quad v_r = 0, \quad \frac{\partial T}{\partial n} = 0; \tag{12}$$

BC 9–12:

$$v_z = v_r = 0, \quad T = T_s. \tag{13}$$

Here v_{avg} is the average gas velocity at the tube inlet, v_z and v_r are the axial and radial gas velocity components, respectively, n is the direction normal to the surface, T_0 is the gas inlet temperature, T_w is the etching chamber wall and tube wall temperature, and T_s is the pedestal temperature. The substrate (wafer) temperature was assumed to be uniform and equal to the pedestal temperature.

BC1 implies a fully developed parabolic gas velocity profile and a spacially uniform gas temperature at the tube inlet. BC2–6 are the no-slip conditions at the solid walls and a constant wall temperature. BC 7,8,13 are the symmetry conditions and reactor exit boundary conditions, and BC 9–12 are the no-slip conditions at the surface of the pedestal and a constant temperature of the pedestal. The extreme case of constant temperature of the walls of the tube and etching chamber may be realized by cooling the walls. The other extreme of zero heat flux normal to the walls is applicable in the case of insulated walls. Practical systems usually operate between these two extremes.
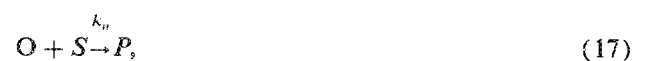
The gas viscosity, heat capacity, and thermal conductivity were expressed as a function of temperature using standard physical property estimation techniques.[26] The above equations provided the flow velocity and temperature distributions in the reactor. Such distributions were then used in the convective diffusion equations describing species transport and reaction as outlined below.

C. Mass transport and reaction

A plethora of neutral and charged species are formed in the plasma region. However, the "activated" gas decays quickly after leaving the discharge cavity and only species with a relatively long lifetime are eventually transported to the etching chamber. Such species include atomic and molecular oxygen and perhaps metastable oxygen and ozone. Nevertheless, metastable oxygen was found not to react with photoresist in a downstream reactor.[27] Moreover, the ozone concentration in the positive column of oxygen dc discharges under conditions comparable to the present work was found to be at least $1\frac{1}{2}$ orders of magnitude lower than the atomic oxygen concentration.[28,29] In addition, ozone is not expected to have much higher reactivity (if at all higher) towards photoresist compared to atomic oxygen. It follows that metastable oxygen and ozone do not appear to be important photoresist etchants. On the other hand, atomic oxygen has been found to be the primary etchant of photoresist under relatively high-pressure (~ 1 Torr) conditions.[30] Therefore, in order to simplify the analysis only three gas-phase species were considered: molecular oxygen, atomic oxygen, and etching reaction product. In general, molecular oxygen is the dominant gas-phase species. Atomic oxygen is produced in the plasma mainly by electron-impact dissociation of molecular oxygen[31] according to reaction equation (3). The reaction rate is $r_p = 2k_p n_e C_2$, where C_2 is the concentration of molecular oxygen. The electron density in the discharge is given by Eq. (2), and n_e was taken to be zero outside the discharge region. The rate constant k_p is given by Eq. (4).

Although not the primary etchants, metastable oxygen and ozone may alter the O-atom balance and hence indirectly influence the etching rate. However, Kaufman[31] and Sabadil and Pfau[28] found wall recombination to be the primary O-atom loss mechanism, at least in the discharge region, at pressures less than about 1 Torr. For higher pressures, volume recombination reactions make a significant contribution to the atomic oxygen balance.[18,19,28] Hence in the present analysis atomic oxygen was assumed to be consumed by volume recombination reactions [Eqs. (14)–(16)], by the etching reaction [Eq. (17)], and by wall recombination [Eq. (18)]:

$$O + O_2 + M \xrightarrow{k_1} O_3 + M, \tag{14}$$

$$O + O + M \xrightarrow{k_2} O_2 + M, \tag{15}$$

$$3O \xrightarrow{k_3} O_2 + O, \tag{16}$$

$$O + S \xrightarrow{k_n} P, \tag{17}$$

$$2O + W \xrightarrow{k_w} O_2 + W. \tag{18}$$

Here k_1, k_2, k_3 are the volume recombination rate constants, M is a third body required to conserve both momentum and

energy during recombination, S represents the photoresist (etching) surface, W represents a wall, P represents the product of the etching reaction, k_n is the etching reaction rate constant, and k_w is the wall recombination rate constant. Volume recombination reactions depend strongly on pressure and are normally negligible below 1 Torr. The volume recombination rate constants were obtained from the literature.[18] In this work, M was assumed to be O_2, the dominant gas-phase species. The wall recombination rate constant was expressed as

$$k_w = \tfrac{1}{4}\gamma u_0, \tag{19}$$

where γ is the wall recombination coefficient, and u_0 is the thermal velocity of the oxygen atoms given by

$$u_0 = \sqrt{8kT/\pi M_1}, \tag{20}$$

where M_1 is the oxygen atom mass. The wall recombination coefficient was assumed to be that of quartz and was obtained as a function of temperature from Graves and Linnett.[32] The etching reaction rate constant was expressed in an Arrhenius form:

$$k_n = k_{n0} \exp(-E/RT_s). \tag{21}$$

The activation energy was taken as $E = 10.7$ kcal/mol,[7,10] which is characteristic of downstream etching of photoresist. The preexponential factor was adjusted such that the etching rate constant agreed with the one calculated from the data of Battey.[33] The resulting value is $k_{n0} = 2.8 \times 10^7$ cm/s.

Mass balance equations were written for O and O_2 neglecting multicomponent diffusion effects and using a pseudobinary diffusion coefficient:

$$\mathbf{v}\cdot\nabla C_i = \nabla\cdot(CD_i\nabla x_i) + G_i. \tag{22}$$

Here C is the total gas concentration, and C_i, x_i, D_i, and G_i are molar concentration, mole fraction, diffusivity, and net production rate of species i, respectively. Subscripts $i = 1$ and $i = 2$ correspond to atomic and molecular oxygen, respectively. The total gas concentration was found by using the ideal gas law

$$C = p/RT. \tag{23}$$

The net production rate of atomic oxygen was written as

$$G_1 = 2k_p n_e C_2 - (k_1 C_1 C_2^2 + 2k_2 C_1^2 C_2 + 2k_3 C_1^3), \tag{24}$$

and that for molecular oxygen was written as

$$G_2 = -k_p n_e C_2 - k_1 C_1 C_2^2 + (k_2 C_1^2 C_2 + k_3 C_1^3). \tag{25}$$

The first term on the right-hand side (rhs) of Eq. (24) is the production of atomic oxygen according to reaction equation (3). The first, second, and third terms in parenthesis on the rhs of Eq. (24) correspond to O-atom elimination reactions according to Eqs. (14), (15), and (16), respectively. Although the production of etchant species is localized in space and occurs in the plasma volume only, etchant volume recombination occurs throughout the reactor volume. The mass balance for the reaction product was not considered since its mole fraction can be found by knowing the other two species mole fractions, and the fact that the sum of the mole fractions must be unity. The O-O_2 binary diffusion coefficient was estimated from experimental collision diameter

data[34] and the O_2 self-diffusion coefficient was estimated using standard methods.[26] Etching and surface recombination reactions enter in the boundary conditions described below. Boundary conditions for Eq. (22) were as follows:
BC1:

$$-D_i C \frac{\partial x_i}{\partial n} = v_z(C_{i0} - C_i); \tag{26}$$

BC2–6,9–11:

$$D_1 C \frac{\partial x_1}{\partial n} = -k_w C_1, \tag{27}$$

$$D_2 C \frac{\partial x_2}{\partial n} = \tfrac{1}{2}k_w C_1; \tag{28}$$

BC12:

$$D_1 C \frac{\partial x_1}{\partial n} = -k_n C_1; \tag{29}$$

BC7,8,13:

$$\frac{\partial x_i}{\partial n} = 0, \tag{30}$$

where C_{i0} is the species concentration in the feed gas, and n is the surface normal pointing outwards the computational domain. Equations (26) and (30) are Danckwerts-type boundary conditions.[35] Equations (27) and (28) represent wall recombination reaction on all surfaces except the etching surface, and Eq. (29) represents etching on the photoresist surface. Simple linear kinetics was assumed for both the wall recombination[32] and the etching reaction.[27,33]

III. METHOD OF SOLUTION

The finite-element method was employed to solve the governing equations. Due to the axisymmetric nature of the system, the computational domain was restricted to only one half of the reactor. The finite-element grid used for most calculations is shown in Fig. 2(a). A large reduction in the required computational effort was achieved by decoupling the fluid flow and heat transport equations from the mass transport equations. Such decoupling is justified at low pressures where, for example, the rate of heat generated by volume recombination reactions is insignificant, and for dilute systems for which the net change in the number of moles upon reaction is negligible.

The coupled fluid flow [Eqs. (5) and (7)] and heat transport [Eq. (9)] equations with the associated boundary conditions were solved first. The penalty function formulation[36,37] was employed to eliminate pressure as one of the dependent variables. The advantages of the method are elimination of one degree of freedom, and reduction of a differential-algebraic equation system to a purely differential equation system. The penalty parameter was selected as $10^8 \mu_0$, where μ_0 is the gas viscosity at the reference temperature T_0.[37] The convective diffusion equations [Eqs. (22)] were solved next using the known fluid velocity and temperature fields.

The streamline upwind Petrov–Galerkin finite-element method[38] was used with bilinear basis functions. The computational domain was divided into 476 elements which led

to 1256 unknowns for the fluid flow/heat transport calculation, and 1160 unknowns for the mass transport calculation. The resulting set of nonlinear algebraic equations was solved using the skyline solver of Gauss elimination with a Newton–Raphson iteration scheme.[39] For a given set of operating conditions, a complete calculation required about 15 mins on a Micro VAXII computer in double precision.

IV. RESULTS AND DISCUSSION

The effect of changes in the reactor design and operating conditions were examined by varying the parameter of interest while keeping other parameters at their basic value. The parameters varied are shown in Table I. Basic parameter values are shown in the third column, and the range of values examined is shown in the last column of Table I. The parameters shown in Table II were not varied. In the calculations that follow, all parameters were at their basic value unless noted otherwise.

Figure 3 shows the temperature distribution in the reactor. The inlet gas and the reactor walls were assumed to be at room temperature ($T_0 = T_w = 298$ K). The pedestal and wafer temperatures were assumed to be $T_s = 373$ K. Owing to the low Reynolds number, the flow is laminar. Due to th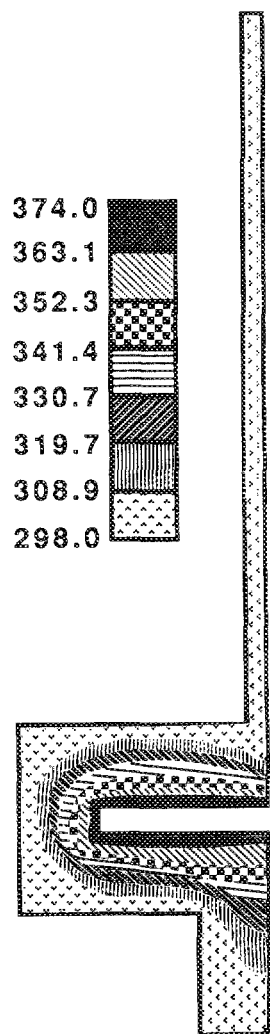e small temperature variations in the reactor, forced convection dominates over buoyancy effects, and no free-convection rolls are observed. Due to the relatively high gas velocity in the tube, the boundary layer is thinner around the stagnation point at the center of the pedestal surface.

Figure 4 shows the concentration distribution (in mole fraction) of atomic oxygen. The atomic oxygen concentration starts with a low value at the tube inlet and increases substantially in the plasma region where O atoms are produced by electron-impact dissociation of O_2 [Eq. (3)]. After leaving the discharge there is no more production of atomic species, and the O-atom concentration in the tube decreases due to volume and wall recombination reactions. The O-atom concentration is further depleted in the etching chamber by the etching reaction as well as by recombination reactions. The recombination reactions are more important in the etching chamber than in the tube because the gas residence time is much shorter in the tube. Hence the atoms have less chance of recombining while in the tube. In the etching chamber, the O-atom concentration is higher around the inlet to the chamber. As the gas flows radially outwards over the wafer, etching and recombination reactions deplete the

FIG. 3. Temperature distribution in the reactor. Parameters were at their basic value (inlet gas $T = 298$ K, pedestal $T = 373$ K).
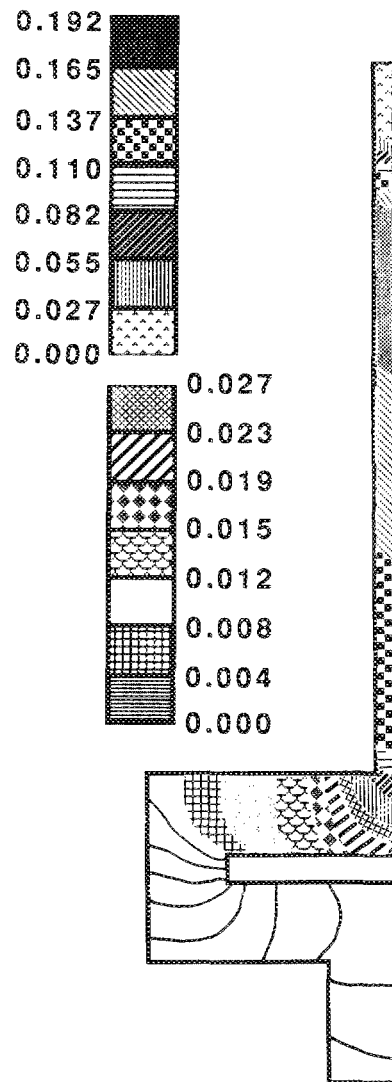

FIG. 4. Concentration distribution of atomic oxygen (mole fraction). Parameters were at their basic value. The upper scale (mole fraction 0.000–0.192) applies to the tube and the entrance region to the etching chamber. The lower scale (mole fraction 0.000–0.027) applies to the rest of the reactor.

O-atoms. The above phenomena lead to higher etching rate at the wafer center. Further, one observes larger concentration gradients around the inlet to the etching chamber, and in the plasma region.

The etching rate was calculated by

$$r_n (\text{Å/min}) = (CF) r_n (\text{mol O/cm}^2 \text{ s}), \tag{31}$$

where the conversion factor is given by

$$CF = \frac{1}{q} \left(\frac{MW_f}{\rho_f} \right) \left(\frac{60}{10^{-8}} \right), \tag{32}$$

and r_n (mol O/cm^2 s) is given by

$$r_n = k_{n0} \exp[(- E/RT_s)] C_1. \tag{33}$$

Here q is the number of moles of atomic oxygen consumed by one mole of the monomeric unit of the polymer (photoresist) film, and ρ_f and MW_f are the film density and molecular weight of the monomer, respectively. The values used were $q = 11, \rho_f = 1.28$ g/cm^3, $MW_f = 94$. These values correspond to etching of a novolak-type photoresist represented by the formula $(C_6H_6O)_n$ assuming that half of the carbon is converted to CO_2 and the other half to CO.[40] The above parameter values are arbitrary but reasonable, and are used here simply to give an idea of what the etching rate in a PADE reactor may be under the conditions examined.

The average etching rate as a function of flow rate is shown in Fig. 5 for different values of power input to the discharge. Other parameters were at their basic value (Table I, third column). The average etching rate was calculated from the local etching rate using

$$r_{\text{avg}} = \frac{2}{R_s^2} \int_0^{R_s} r_n r \, dr. \tag{34}$$

The etching rate raises quickly with flow rate in the low flow-rate regime, reaches a maximum, and then decreases slowly in the high flow-rate regime. At low flow rates, the gas residence time in the tube and in the etching chamber is large and the chance for etchant species recombination is high. This results in lower etchant concentration over the wafer and hence lower etching rate. Further, at low flow rates, the process is limited by the reactant supply. At very high flow rates, the chance for etchant recombination is low, but the gas residence time in the plasma region is low as well. Hence the degree of dissociation of the gas in the plasma is small, again resulting in lower etching rate. Therefore, the etching rate is maximum at an intermediate flow rate. The location of the maximum depends on the reactor design and operating conditions, especially pressure (see discussion of Fig. 7 below). The effect of flow rate is more pronounced for higher values of power.

The etching rate distribution along the wafer radius is shown in Fig. 6 for different input gas flow rates. At low flow rates (e.g., 50 sccm) diffusion is important in species transport. Hence the resulting concentration gradients are mild and etching uniformity is improved. At higher flow rates (e.g., 300 sccm) convection dominates diffusion and the etching rate is substantially higher at the wafer center where "fresh" reactant first encounters the etching film. At even higher flow rates (e.g., 1000 sccm) the reactant depletion is not appreciable as the gas flows over the etching surface.
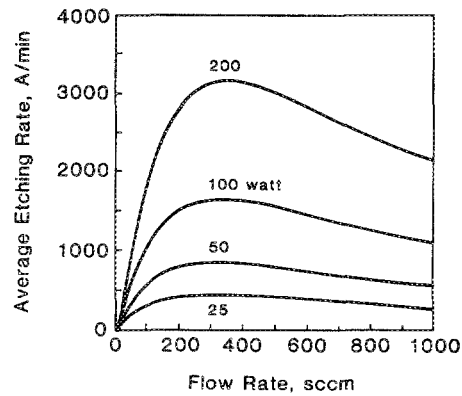
FIG. 5. Average etching rate as a function of gas flow rate for different values of power. Other parameters were at their basic value.

This results in improved uniformity again. The uniformity index was defined as

$$UI = (r_{\text{max}} - r_{\text{min}})/2r_{\text{avg}}, \tag{35}$$

where r_{max} is the maximum etching rate, r_{min} is the minimum etching rate, and r_{avg} is the average etching rate. The higher the uniformity index, the worse the etching uniformity (higher nonuniformity). Under the conditions of Fig. 6, the uniformity index was found to increase with flow rate up to 300 sccm, and then decrease with flow rate.

The average etching rate as a function of pressure is shown in Fig. 7 for different values of gas flow rate. At low pressure, the molecular oxygen concentration is low and the gas residence time in the plasma region is small (flow rate is kept constant while the pressure varies). These two effects more than compensate for the increase in electron density and energy in the plasma with decreasing pressure. The net result is low etchant concentration and low etching rates. At higher pressure, etchant production in the plasma is more effective, yet recombination reactions are still unimportant. Hence the etching rate increases. At still higher pressure the electron density and energy in the discharge decrease markedly and volume recombination reactions come into play. Hence the etching rate decreases in the high pressure regime.
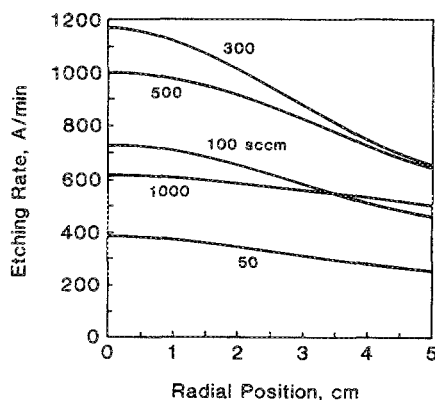
FIG. 6. Etching rate as a function of radial position along the wafer for different values of gas flow rate. Other parameters were at their basic value.
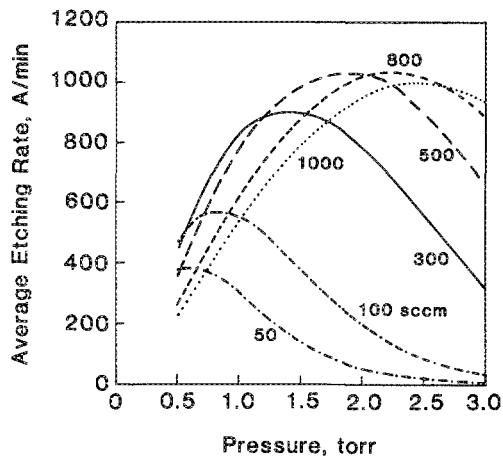
FIG. 7. Average etching rate as a function of gas pressure for different values of gas flow rate. Other parameters were at their basic value.

FIG. 9. Average etching rate as a function of power for different gas pressures. Other parameters were at their basic value.

The maximum in etching rate with pressure depends strongly on the flow rate as seen in Fig. 7. The higher the flow rate, the higher the optimum pressure to maximize the etching rate. For example, for a flow rate of 100 sccm, the optimum pressure is around 0.75 Torr, but for 1000 sccm, the optimum pressure is around 2.5 Torr. A maximum in the etching rate as a function of flow rate was observed experimentally by Spencer et al.[7] and this maximum was found to be pressure dependent.

The etching rate distribution along the wafer radius for different values of pressure is shown in Fig. 8. Other parameters were kept at their basic value. At low pressure (0.5 Torr) etchant diffusivity is high and volume recombination is low, yielding small concentration gradients and better uniformity. At higher-pressure large concentration gradients develop leading to nonuniform etching. In fact, the uniformity index increases monotonically with pressure, indicating a degradation of uniformity with increasing pressure.

The average etching rate as a function of power for different values of gas pressure is shown in Fig. 9. As power increases, the electron density in the discharge increases re-

sulting in higher gas dissociation rate and hence higher etching rate. The dependence of etching rate on power is nearly linear at low-power values but turns into sublinear at high-power values, especially in the high-pressure regime. This is due to the nonlinear volume recombination reactions becoming more important at higher power (higher etchant concentration) and higher pressure. The effect of power on the uniformity index was found to be rather weak especially in the low-pressure (<1 Torr), high flow-rate (>300 sccm) regime. The nearly linear dependence of etching rate on power has been observed experimentally by Dzioba et al.[6]

The dependence of the average etching rate on substrate temperature is shown by the Arrhenius-type plot of Fig. 10. The pedestal temperature was the same as that of the substrate. The etching rate constant was that given by Eq. (21). In addition, the temperature dependence of the recombination coefficient on the pedestal surface was taken into account. At low temperature the process is kinetically controlled and the activation energy is that of the etching reaction. At high temperature, however, the process is limited by etchant diffusion to the wafer surface and the etching
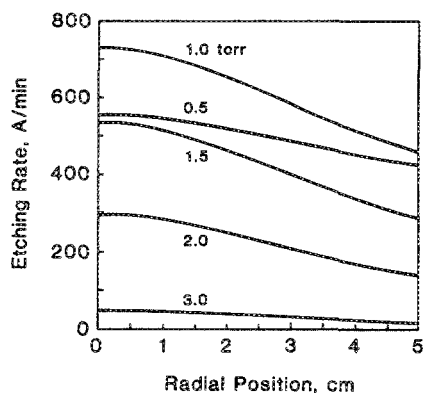

FIG. 8. Etching rate as a function of radial position along the wafer for different values of gas pressure. Other parameters were at their basic value.
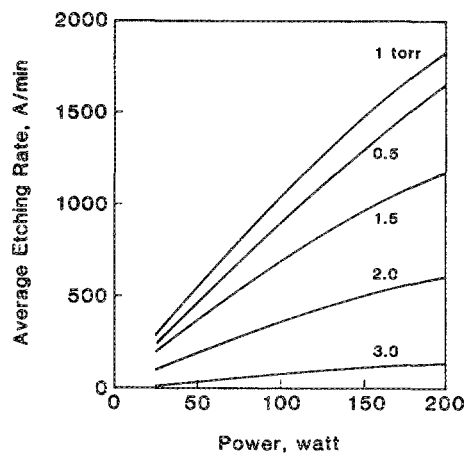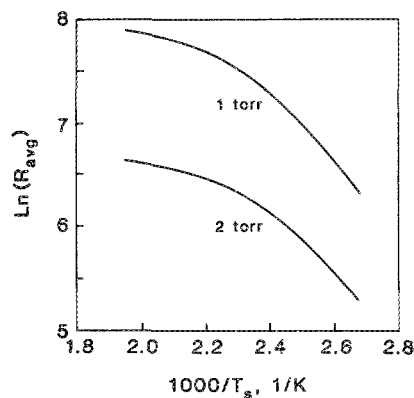

FIG. 10. Logarithm of the average etching rate as a function of the inverse of the wafer temperature for two different gas pressures. Other parameters were at their basic value.

rate becomes relatively insensitive to temperature. When plotting experimental data to derive the reaction apparent activation energy, one has to make certain that diffusional limitations do not play a role in the process. In addition, one needs to be concerned with the fact that the bulk etchant concentration may change as a result of a change in the substrate temperature. This is due to the loading effect which is present if the etching reaction is an important sink of active species.

The etching rate distribution along the wafer radius is shown in Fig. 11 for different values of the substrate temperature. At low temperature, the etching rate is higher at the wafer center and decreases monotonically towards the wafer edge, as observed earlier (see Fig. 6). At high temperature, however, the etching rate shows a minimum close to the wafer edge. This is a result of rapid consumption of etchant species on the wafer surface compared to slower consumption on the pedestal surface surrounding the wafer. Thus, etchant species diffuse towards the wafer from the relatively inert surrounding areas, yielding a higher etchant concentration at the wafer edge and a higher etching rate there. This local loading effect is similar to that observed in parallel-plate plasma etching reactors.[41] Moreover, under the conditions examined, the uniformity index was found to increase rapidly with temperature above 400 K, implying greater nonuniformity at higher temperature.

Since active species recombine during their transit from the plasma region to the etching chamber, the etching rate can be made higher by placing the substrate closer to the plasma. However, the minimum permissible substrate-plasma distance will be dictated by the decay time of the afterglow gas so that radiation damage is avoided. Furthermore, the substrate temperature may be difficult to control when the substrate is near the plasma. Figure 12 is a semilogarithmic plot of the average etching rate as a function of the plasma end to substrate distance [H_{ps}, see Fig. 2(b)] for different gas pressures. At low pressure (0.5 Torr) the etching rate decreases only slightly with distance since volume recombination reactions are negligible. At high pressure there is a dramatic decrease in etching rate with distance from the

FIG. 12. Logarithm of the average etching rate as a function of distance from the plasma end to the substrate (H_{ps}) for different values of gas pressure. Other parameters were at their basic value.

plasma because of volume recombination of the etchant species. Figure 12 also shows that the optimum pressure for maximizing the etching rate depends on the distance from the plasma. For example, for a distance of 40 cm, the maximum etching rate is achieved at a pressure of 0.75 Torr (see also Fig. 7). However, as seen in Fig. 12, the maximum etching rate is achieved at around 1.5 Torr for a distance of 10 cm. The dependence of etching rate on distance from the plasma has been observed experimentally to follow the behavior shown in Fig. 12.[6,9]

The decay of the O-atom concentration in the afterglow in tubular reactors has been analyzed.[42,43] However such analyses are not applicable to the problem at hand since no account is taken for the presence of etchable substrate. Owing to the loading effect, the O-atom concentration depends on the reactivity of the substrate as well as the substrate area. Moreover, the above analyses are not capable of predicting etching uniformity.

The effect of distance between the substrate and tube-exit (H_{ts}) is shown in Fig. 13. As the distance decreases the etching rate increases. This is because of the shorter gas resi-
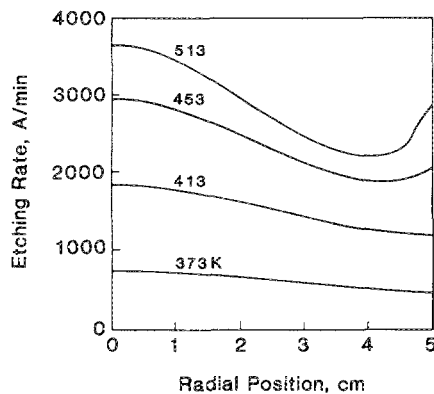

FIG. 11. Etching rate as a function of radial position along the wafer for different wafer temperatures. Other parameters were at their basic value.
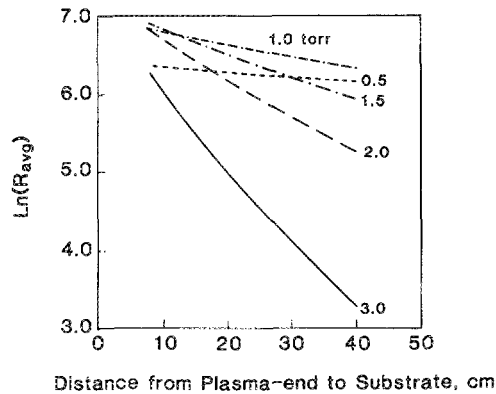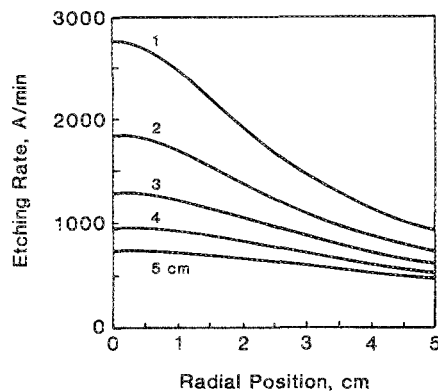

FIG. 13. Etching rate as a function of radius along the wafer for different values of the distance between tube end and substrate (H_{ts}). Other parameters were at their basic value.

dence time in the etching chamber, resulting in lesser recombination and higher O-atom concentration. Further, the mass transfer boundary layer thickness at the stagnation point (at $r = 0$) decreases as the substrate moves closer to the tube exit. Although the average etching rate improves by positioning the substrate near the tube exit, such action results in significantly worse etching uniformity, because the gas distribution over the wafer becomes more nonuniform. The etching uniformity may improve, while preserving the etching rate, by providing for a more uniform gas-flow distribution over the wafer surface. This may be accomplished by tapering the wall near the tube exit as shown by the dashed line in Fig. 2(b). Another method to achieve similar results is to use a porous disk, perhaps with diameter equal to the wafer diameter, which showers the gas uniformly over the wafer surface, much the same way as in single-wafer plasma etchers of the showerhead-electrode configuration.[41]

The effect of wall tapering is shown in Fig. 14. Conditions were otherwise the same as in Fig. 13. One observes an improvement in the etching uniformity with only a moderate reduction in the etching rate. The increased uniformity is brought about by the more uniform gas-flow distribution over the etching surface.

Increasing the radius all along the tube length resulted in improved etching uniformity, again due to the more uniform gas distribution over the wafer. At the same time the etching rate decreased, however, due to the longer gas residence time in the tube and the increased importance of recombination reactions.

The above analysis reveals that etching rate and uniformity may be optimized simultaneously by choosing reactor operating conditions which promote efficient gas dissociation in the plasma, rapid transport of the dissociated gas to the etching chamber to minimize active species recombination, and uniform gas distribution over the wafer to improve etching uniformity. However, for a given reactor geometry, selection of the operating conditions to satisfy all of the above requirements may be difficult. For example, rapid transport of the dissociated gas necessitates high gas-flow rate, which however results in a low gas residence time in the plasma and inefficient gas dissociation. This suggests that
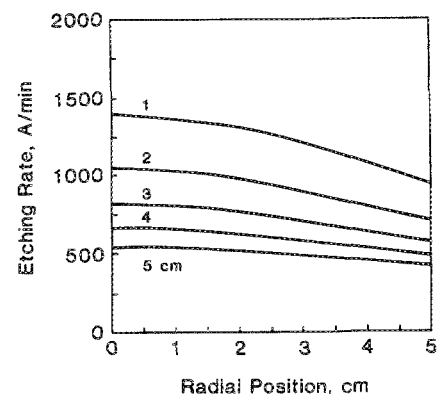
alternative reactor designs may be deviced to alleviate such opposing factors. For instance, the diameter of the tube in the plasma region may be made larger than the diameter of the rest of the tube. This will allow for longer gas residence time in the plasma to achieve higher gas dissociation, and at the same time rapid transport of the dissociated gas to the etching chamber. A reactor with such a design change is also shown in Fig. 2(b). The new reactor differs from the "basic" configuration (solid line) in that it has a tapered wall at the entrance to the etching chamber (dashed line) and a 2-cm radius of the plasma cavity (dash-dotted line). The performance of such a reactor in terms of etching rate and uniformity (Fig. 15, line C) is compared to the "basic" reactor geometry (line A), and to the one with tapered walls but with a 1-cm radius of the plasma cavity (line B). Other parameters were at their basic value. One observes a remarkable improvement in both the etching rate and uniformity using the new reactor design.

In the above analysis, the plasma length H_p [see Fig. 2(b)] was assumed constant independent of reactor operating conditions. However, the extend of the plasma depends on the operating conditions especially pressure and power. For example, the plasma expands at lower pressures because of the higher diffusivity of the plasma electrons. Theoretical prediction of the plasma length is difficult and beyond the scope of the present work. However, in order to assess the effect of plasma length on etching rate and uniformity, simulations were conducted varying the plasma length in the range 2–8 cm, while keeping the other parameters at their basic value (Table I). It was found that both etching rate and uniformity were affected by less than 5%. This result can be explained as follows. As the plasma expands, for instance, the electron density falls and hence the atom production rate decreases. However, the gas residence time in the plasma increases resulting in higher dissociation. Apparently, the two effects nearly balance each other especially for locations far downstream from the plasma. From the above analysis it can be concluded that changes in the plasma volume with reactor operating conditions are of secondary im-

FIG. 14. Etching rate as a function of radius along the wafer for different values of the distance between tube end and substrate (H_b) in the reactor with tapered walls. Other parameters were at their basic value.
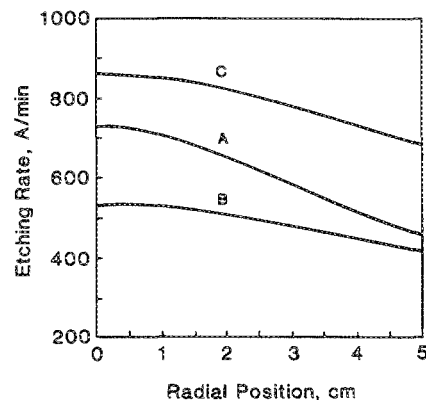

FIG. 15. Comparison of three reactor designs in terms of the etching rate along the wafer radius. Line A: Basic reactor configuration [see Fig. 2(b), solid line]. Line B: Reactor with tapered walls [see Fig. 2(b), dashed line]. Line C: Reactor with tapered walls and with a 2-cm radius of the plasma region [see Fig. 2(b), dash-dotted line].

portance in describing etching rate and uniformity in the system studied.

V. SUMMARY AND CONCLUSIONS

A two-dimensional mathematical model was developed for a plasma-assisted downstream etching (PADE) reactor of the impinging jet configuration. Finite-element methods were employed to solve for the coupled fluid velocity and temperature fields, and in turn for the concentration distribution of active species. Etchant production and both volume and wall recombination of etchant were included. Etching of polymer (e.g., photoresist) in a pure oxygen plasma was chosen as a model system for analysis. The rationale for such choice was that the oxygen discharge is relatively better understood, and that stripping of photoresist using oxygen plasmas is currently the primary application of downstream etching reactors. To our knowledge, this is the first relatively detailed model of a PADE reactor.

The effect of reactor design and operating conditions on the etching rate and uniformity was analyzed. Parameter values in the range typical of practical systems were selected. The effect of power input to the discharge, gas pressure and flow rate, substrate temperature, distance between the plasma and the substrate, and reactor geometry were examined. For given power and gas flow rate, optimum values of the gas pressure were identified that maximized the etching rate. The location of the optimum pressure depended strongly on flow rate and shifted to higher pressure at higher flow rate. The optimum pressure also depended on the distance between the plasma and the substrate, shifting to higher pressure as that distance decreased. For given pressure, the etching rate increased linearly with power at low-power values, but the dependence turned into sublinear at higher-power values, especially in the high-pressure regime. The etching rate decreased nearly exponentially with distance between the plasma and the substrate.

Under the conditions examined, the etching rate was always found to be highest at the wafer center. The etching rate decreased monotonically towards the wafer edge, except for high temperatures for which a minimum in the etching rate was observed near the wafer edge. This behavior was attributed to the flow distribution in the impinging jet reactor configuration and to a local loading effect manifested at high temperatures. The etching uniformity was found to improve (low uniformity index) at low pressure and low substrate temperature. Increasing the flow rate initially resulted in worse uniformity, but further increase in the flow rate resulted in improved uniformity. Power was found to have little effect on uniformity. Hence, since etching rate increases monotonically with power, one should operate at the highest possible power compatible with other system constraints. Etching uniformity was found to depend on the gas-flow distribution over the wafer surface and on the distance between the wafer and the tube end (inlet to the etching chamber). A reactor with tapered walls at the tube end yielded much improved uniformity compared to a reactor with straight walls, with only a moderate reduction in the etching rate.

Based on the parametric investigation of the system, a new reactor design was proposed which featured effective gas dissociation in the plasma region, rapid transport of the dissociated gas to the etching chamber, and nearly uniform gas distribution over the wafer surface. The new reactor resulted in remarkable improvement in both the etching rate and uniformity.

The present mathematical model was based on several assumptions and on a simplified treatment of the gas discharge. For example, the dilute mixture approximation was made in order to decouple the fluid flow and heat transport equations from the mass transport equations. Such decoupling led to substantial savings in computational time. Furthermore, the electron density and temperature in the plasma were derived from an approximate discharge model assuming pure oxygen, and changes in plasma gas temperature with power and pressure were neglected. Nevertheless, the above approximations and assumptions appear to be justified over a wide range of operating conditions of the PADE reactor. The approximations are better in the low-power, low-pressure, and high flow-rate regime. The present mathematical model may be used to analyze other PADE systems for which chemical reaction data exist. An example is the etching of polymer or silicon using a CF_4/O_2 plasma.[44] Further, a similar model may be used to analyze plasma-assisted downstream deposition reactors. A problem not addressed in the present work is the charged species decay in the afterglow. The solution to this problem requires a detailed reaction scheme including electrons, positive and negative ions, and neutrals. For the plasma-substrate distance used in the present work, it is expected that the charged species decay before reaching the substrate.

Unfortunately, experimental data taken under the conditions of the system studied could not be found to perform a quantitative comparison with the model predictions. Such comparison, if successful, would greatly enchance one's confidence in the predictive capabilities of the model.

The behavior of plasma-assisted downstream etching reactors is governed by the complex interdependence of plasma physical chemistry, heat and mass transport, chemical reactions, and fluid flow in complicated geometries. For this reason, it is difficult to predict the reactor behavior based on intuition alone. Further, trial-and-error experimentation to optimize a given process is usually costly and time consuming. Mathematical models based on the fundamental principles of the process may be useful tools in reactor design, process control, and optimization.

[1]G. S. Oehrlein, S. W. Robey, J. L. Lindstrom, K. K. Chan, M. A. Jaso, and G. J. Scilla, *Proceedings of the 7th Symposium on Plasma Processing*, edited by G. S. Mathad, G. C. Schwartz, and D. W. Hess (The Electrochemical Society, Pennington, NJ, 1988), Vol. 88–22, p. 151.

[2]S. J. Fonash, Solid State Technol., 201 (1985).

[3]H. Akiya, K. Saito, and K. Kobayashi, Jpn. J. Appl. Phys. 20, 647 (1981).

[4]S. Fujimur and H. Yano, J. Electrochem. Soc. 135, 1195 (1988).

[5]A. Kalnitsky and W. K. Chung, J. Electrochem. Soc. 135, 2338 (1988).

[6]S. Dzioba, G. Este, and H. M. Naguib, J. Electrochem. Soc. 129, 2537 (1982).

[7]J. E. Spencer, R. A. Borel, and A. Hoff, J. Electrochem. Soc. 133, 1922 (1986).

[8]V. Vukanovic, G. A. Takacs, E. A. Matuszak, F. D. Egitto, F. Emmi, and R. S. Horwath, J. Vac. Sci. Technol. B 6, 66 (1988).

[9]J. J. Hannon and J. M. Cook, J. Electrochem. Soc. 131, 1164 (1984).

[10]L. M. Loewenstein, C. H. Huffman, and C. J. Davis, Mater. Res. Soc. Symp. Proc. 98, 267 (1987).

[11]L. Loewenstein, J. Vac. Sci. Technol. A 6, 1984 (1988).

[12]G. Smolinsky and D. L. Flamm, J. Appl. Phys. 50, 4982 (1979).

[13]S. Suto, N. Hayasaka, H. Okano, and Y. Horiike, in *Proceedings of the Symposium on Dry Process*, edited by J. Nishizawa, Y. Horiike, M. Hirose, and K. Suto (The Electrochemical Society, Pennington, NJ, 1988), Vol. 88–7, p. 86.

[14]T. Ono, M. Oda, C. Takahashi, and S. Matsuo, J. Vac. Sci. Technol. B 4, 696 (1986).

[15]R. A. Rudder, G. G. Fountain, and R. J. Markunas, J. Appl. Phys. 60, 3519 (1986).

[16]G. Lucovsky, P. D. Richard, D. V. Tsu, S. Y. Lin, and R. J. Markunas, J. Vac. Sci. Technol. A 4, 681 (1986).

[17]D. J. Vitkavage, R. A. Rudder, G. G. Fountain, and R. J. Markunas, J. Vac. Sci. Technol. A 6, 1812 (1988).

[18]A. T. Bell, in *Techniques and Applications of Plasma Chemistry*, edited by J. R. Hollahan and A. T. Bell (Wiley, New York, 1974), p. 1.

[19]J. W. Dettmer, Ph.D. thesis, Air Force Institute of Technology, 1978.

[20]J. S. Townsend, Philos. Mag. xxvi, 290 (1938).

[21]B. E. Cherrington, *Gaseous Electronics and Gas Lasers* (Pergamon, Oxford, 1979).

[22]D. J. Economou and R. C. Alkire, J. Electrochem. Soc. 135, 2786 (1988).

[23]J. E. Heidenreich III, J. R. Paraszczak, M. Moisan, and G. Sauve, J. Vac. Sci. Technol. B 6, 288 (1988).

[24]G. Sauve, M. Moisan, J. Paraszczak, and J. Heidenreich, Appl. Phys. Lett. 53, 470 (1988).

[25]H. Schlichting, *Boundary-Layer Theory*, 7th ed. (McGraw-Hill, New York, 1979).

[26]R. C. Reid, J. M. Prausnitz, and T. K. Sherwood, *The Properties of Gases and Liquids*, 3rd ed. (McGraw-Hill, New York, 1977).

[27]J. M. Cook and B. W. Benson, J. Electrochem. Soc. 130, 2459 (1983).

[28]H. Sabadil and S. Pfau, Plasma Chem. Plasma Process. 5, 67 (1985).

[29]G. Gousset, P. Panafieu, M. Touzeau, and M. Vialle, Plasma Chem. Plasma Process. 7, 408 (1987).

[30]M. A. Hartney, D. W. Hess, and D. S. Soane, J. Vac. Sci. Technol. B 7, 1 (1989).

[31]F. Kaufman, in *Chemical Reactions in Electrical Discharges*, Advances in Chemistry Series (ACS, Washington, DC, 1969) Vol. 80, p. 29.

[32]J. C. Graves and J. W. Linnett, Trans. Faraday Soc. 55, 1355 (1959).

[33]J. F. Battey, J. Electrochem. Soc. 124, 437 (1977).

[34]R. A. Young, J. Chem. Phys. 34, 1295 (1961).

[35]P. V. Danckwerts, Chem. Eng. Sci. 2, 1 (1953).

[36]J. N. Reddy, Int. J. Num. Methods Fluids 2, 151 (1982).

[37]T. J. R. Hughes, W. K. Liu, and A. Brooks, J. Comput. Phys. 30, 1 (1979).

[38]A. N. Brooks and T. J. R. Hughes, Comput. Methods Appl. Mech. Eng. 32, 199 (1982).

[39]T. J. R. Hughes, *The Finite Element Method* (Prentice-Hall, Englewood Cliffs, NJ, 1987).

[40]R. F. Reichelderfer, J. M. Welty, and J. F. Battey, J. Electrochem. Soc. 124, 1926 (1977).

[41]D. J. Economou, S.-K. Park, and G. Williams, J. Electrochem. Soc. 136, 188 (1989).

[42]P. D. Francis, Brit. J. Appl. Phys. (J. Phys. D), Ser. 2 2, 1717 (1969).

[43]M. L. Brake and R. L. Kerber, Plasma Chem. Plasma Process. 3, 79 (1983).

[44]I. C. Plumb and K. R. Ryan, Plasma Chem. Plasma Process. 6, 205 (1986).